A compact 6D suction cup model for robotic manipulation via symmetry reduction

Alexander Oliva, Maarten Johannes Jongeneel, Alessandro Saccon

A compact 6D suction cup model for robotic manipulation via symmetry reduction

Alexander A. Oliva , Maarten J. Jongeneel and Alessandro Saccon

***Abstract*—Active suction cups are widely adopted in industrial and logistics automation. Despite that, validated dynamic models describing their 6D force/torque interaction with objects are rare. This work aims at filling this gap by showing that it is possible to employ a compact model for suction cups, providing good accuracy also for large deformations. Its potential use is for advanced manipulation planning and control. We model the interconnected object-suction cup system as a lumped 6D mass-spring-damper systems, employing a potential energy function on $\mathbf{SE}(3)$, parametrized by a 6×6 stiffness matrix. By exploiting geometric symmetries of the suction cup, we reduce the parameter identification problem, from $6(6+1)/2 = 21$ to only 5 independent parameters, greatly simplifying the parameter identification procedure, that is otherwise ill-conditioned. Experimental validation is provided and data is shared openly to further stimulate research. As an indication of the achievable pose prediction in steady state, for an object of about 1.75 kg, we obtain a pose error in the order of 5 mm and 3 deg, with a gripper inclination of 60 deg.**

***Index Terms*—Modeling, Robotics, Manipulation, Suction cup, Parameters identification, Symmetry, Logistics.**

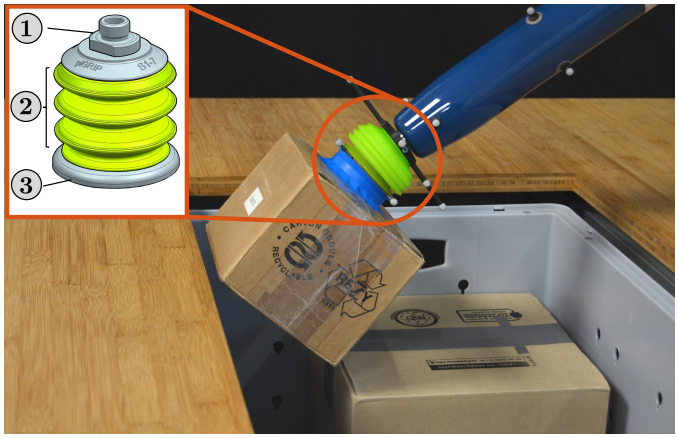

Fig. 1: Example of a robotic bin-to-bin application where the deformation of an active bellow suction cup is clearly visible. Our proposed model allows to accurately predict this deformation enabling new robotic manipulation tasks.The particular shows the parts of a suction cup: 1) Fitting 2) Bellows 3) Lip.

I. Introduction

SUCTION CUPS are the most widely used manipulation end-effectors in the automation industry [1]. The reason for this success is that they are highly customizable, have a quick gripping response, and are capable of delicately handling a wide variety of objects of different materials, weights, and shapes, even in the presence of curved or flexible surfaces, like filled plastic bags or films. Furthermore, suction cups have the potential to be used as soft fingertips to perform several manipulation tasks such as pushing [1], toppling [2], or dragging [3], because their suction ability enables a bilateral contact and permits them to pull in addition to push. Examples of robotics applications where suction cups have recently been employed include bin picking [4], [5], [6], bin packing [7], order fulfillment [8], [3], [9], depalletizing [10], automated trash-sorting [11] or even wall-climbing [12], [13].

Since a seminal work describing the design, kinetostatic, and safety analysis of a mobile wall-climbing robot equipped with suction cups on the legs [12], much effort has been devoted to the modeling and simulation of suction cups for robotic applications. A mathematical model for determining the normal and tangential contact pressures between suction cup and a flat object, with the objective of finding the minimum value of the static friction coefficient and the vacuum level that guarantees a firm grasp, was developed for both a single [14] and multiple [15] square suction cups. More recent works on the subject have emerged proposing a compliant suction contact model employing quasi-static spring assumptions to quantify the seal formation [4]. In [1], a locally-linear force-deformation model that is fitted online starting from a deformation-reaction force dataset pre-recorded from a Force/Torque sensor allows to compute an estimate of the suction cup deformation from the measured wrench; The model is then used for control purposes. A study focusing on the maximum forces that prevent suction cup detachment while moving an object in fast pick and place operations is presented in [16]. A linear visco-elastic model to describe the suction cup during contact in fast vertical picking is detailed in [17]. Active-vacuum suction cups in dynamic holding conditions are also studied in [5] with the goal of improving energy efficiency in handling processes. There, the authors considers the 1D dynamic deformation behavior of vacuum grippers in interaction with a specific gripper-object combination imposing a predetermined force-deformation stiffness model whose parameters are then learned from quasi-static experiments. A parametric position-dependent nonlinear damping model is then tuned by means of pull-off experiments conducted at different velocities. A thorough physics-based model using a constraint-based FEM simulation to describe the suction phenomenon of a suction cup is reported in [18]. One of the most

This work was partially supported by the Research Project I.AM. through the European Union H2020 program under GA 871899. The authors are with the Department of Mechanical Engineering, Eindhoven University of Technology (TU/e), The Netherlands {a.a.oliva, m.j.jongeneel, a.saccon}@tue.nl

recent papers published on the subject [19], proposes a static model with no damping, while recognises the urgent need of developing validated suction cup models and implementing them in physics simulators to enable a step change in robotics manipulation capabilities.

For manipulation purposes, such as in the robotic bin-to-bin application depicted in Fig. 1, it is paramount to forecast the pose of the package held by the suction cup, and hence the suction cup's deformation. Modeling attempts to capture the visco-elastic behaviour of the suction cup (or a system of suction cups) can be found in [5], [20] and references therein. What [5] refers to as the "standard model", is a generalized Kelvin–Voigt model (a parallel connection of spring and damper) which is implemented only for the axial direction, while [20] implemented it on two degrees of freedom. To the best of the author's knowledge, there is no literature reporting model-based or data-driven models to predict the 6D *object-suction cup* interaction in dynamic settings.

The present work takes a first step in this direction proposing a 6D model describing the interaction forces between the suction cup and the held object. The coupled *object-suction cup* body is modeled as a *mass-spring-damper* system, while taking a different approach from [5], [20]. In this paper, the spring wrench is thoroughly investigated and its symmetries exploited. For the sake compactness, the details of the derivation of the damping wrench will be the subject of a future publication. The main contributions made by this paper can be summarized as follows:

1) A coupled 6D linear-torsional model of the object-suction-cup interconnection during holding, written using rotation matrices and guaranteeing its passivity as it is derived from a potential energy, following the seminal work [21] on lumped modeling of elastic bodies.
2) A simplified model employing only 5 parameters instead of the original $6(6+1)/2 = 21$ ones, obtained making use of the newly introduced mathematical model, axial symmetry and in-plane wrench-deformation constraint, allowing for a robust parameter identification and economical data-collection.
3) An open dataset containing 1200 static pose measurements of the deformation of a commercially available bellow suction cup under different payloads, for reproducibility and to further stimulate research on suction-cup modeling.

The modeling and parameter identification procedure on the reduced-order parameter model is validated by means of motion capture (mocap) data and the model's prediction capability is demonstrated by means of numerical simulations.

II. Preliminaries

Let consider the system depicted in Fig. 1, consisting of the blue tool-arm (TA) and the package (PA), modeled as rigid bodies, interconnected by mean of a flexible body: the suction cup (SC). Three main phases can be distinguished when manipulating objects with a suction cup: the ***contact*** (when the suction cup impacts the package), the ***holding*** (when the suction cup uses the vacuum to carry a package) and the ***release*** phase (where the vacuum is deactivated and pressurized air is injected in the suction cup to quickly release the package [22]). Each of these phases requires a different model. In this paper, we devise a compact model describing the suction cup - package interaction during the *holding phase*.

A. Notation for rigid transformations

This subsection introduces the notation employed in the paper. It can be skimmed through at first read and consulted in a later stage when needed. Coordinate frames are indicated with capital letters (A, B, ...) and further specified by indicating their origin ($\mathbf{o}_A$, $\mathbf{o}_B$, ...) and orthogonal unit vectors ($\boldsymbol{x}_A$, $\boldsymbol{y}_A$, and $\boldsymbol{z}_A$ for frame A, $\boldsymbol{x}_B$, $\boldsymbol{y}_B$, and $\boldsymbol{z}_B$ for frame B, ...) [23]. As example, for a frame A, we will write its origin as $\mathbf{o}_A$ and its orientation frame as $[A]$ such that $A = (\mathbf{o}_A, [A])$. Points are indicated with a bold letter such as $\mathbf{p}$ (or $\mathbf{o}$ when corresponding to a coordinate frame's origin) with a suitable subscript for differentiating them. A coordinate vector with respect to a frame of reference is indicated with a left superscript so that, e.g., ${}^A\mathbf{p}$ are the coordinates of $\mathbf{p}$ expressed in A and ${}^B\mathbf{p}$ are the coordinates of the same point $\mathbf{p}$ but now expressed in B. We write a rigid-body's pose using the homogeneous transformation matrix such that

$$ {}^A\mathbf{H}_B = \begin{bmatrix} {}^A\mathbf{R}_B & {}^A\mathbf{o}_B \\ \mathbf{0}_{1\times 3} & 1 \end{bmatrix} \in \mathrm{SE}(3) \tag{1} $$

is a transformation matrix with ${}^A\mathbf{R}_B \in \mathrm{SO}(3)$ a rotation matrix and ${}^A\mathbf{o}_B \in \mathbb{R}^3$ the origin of frame B fixed to the object expressed in terms of frame A. Furthermore, with

$$ {}^A\mathbf{v}^\wedge_{A,B} = \begin{bmatrix} {}^A\boldsymbol{v}_{A,B} \\ {}^A\boldsymbol{\omega}_{A,B} \end{bmatrix}^\wedge := \begin{bmatrix} {}^A\boldsymbol{\omega}^\wedge_{A,B} & {}^A\boldsymbol{v}_{A,B} \\ \mathbf{0}_{1\times 3} & 0 \end{bmatrix} \in \mathfrak{se}(3) \tag{2} $$

we denote the relative velocity (twist) of frame B with respect to A, expressed in the coordinated of A. In (2), we use $\wedge$ (hat) to indicate the classical mapping from $\mathbb{R}^3$ to the corresponding 3×3 skew-symmetric matrix in $\mathfrak{so}(3)$ that represents the matrix form of the cross-product in $\mathbb{R}^3$, and is such that given two vectors $\boldsymbol{\omega}, \boldsymbol{u} \in \mathbb{R}^3$, $\boldsymbol{\omega}^\wedge \boldsymbol{u} = \boldsymbol{\omega} \times \boldsymbol{u}$. Similarly, we use $\vee$ (vee) as the inverse mapping [24, Chapter 3.2]. We recall that given $\mathbf{R} \in \mathrm{SO}(3)$, the $\log(\mathbf{R}) = \boldsymbol{\omega}^\wedge \in \mathfrak{so}(3)$, where $\log$ denotes the matrix logarithm, which can be effectively computed using the inverse of Rodriques formula [25, Section 3.2.3.3]. Note that both ${}^A\mathbf{H}_B$ and ${}^A\mathbf{v}_{A,B}$ in (1) and (2), respectively, are written as $\mathbb{R}^{4\times4}$ matrices. In Lie group theory, the logarithmic map of a Lie group $\mathrm{SE}(3)$ transfers elements from the Lie group to its tangent space $\mathfrak{se}(3)$, which is denoted with $T_{\mathbf{H}}\mathrm{SE}(3)$. The coordinates of a wrench (vector of forces and moments $\boldsymbol{f}, \boldsymbol{\tau} \in \mathbb{R}^3$) with respect to a given frame B are indicated as

$$ {}_B\mathbf{f} = \begin{bmatrix} {}_B\boldsymbol{f} \\ {}_B\boldsymbol{\tau} \end{bmatrix} \in \mathbb{R}^6. \tag{3} $$

The notation can be further specialized with the use of the subscript $BD1 \to BD2$ to specify that the wrench is acting from body $BD1$ on body $BD2$ (${}_B\mathbf{f}_{BD1\to BD2}$).

Given an homogeneous matrix ${}^B\mathbf{H}_S$, its associated adjoint matrix ${}^B\mathbf{X}_S \in \mathbb{R}^{6\times6}$ allows to project a *twist* (in vector form $\in \mathbb{R}^6$) expressed in frame S into frame B while its dual ${}_B\mathbf{X}^S$ allows to project a *wrench* expressed in frame S into frame B.

The following relationship holds between the adjoint matrix and its dual

$$ {}_B\mathbf{X}^S = {}^S\mathbf{X}_B^\top = \begin{bmatrix} {}^B\mathbf{R}_S & \mathbf{0}_{3\times3} \\ {}^B\mathbf{o}_S^\wedge {}^B\mathbf{R}_S & {}^B\mathbf{R}_S \end{bmatrix}. \tag{4} $$

Finally, the $\bar{\times}^*$ operator represents the dual cross-product between a twist and a wrench, and is defined as

$$ {}^B\mathbf{v}_{A,B}\bar{\times}^* = \begin{bmatrix} {}^B\boldsymbol{\omega}_{A,B}^\wedge & \mathbf{0}_{3\times3} \\ {}^B\boldsymbol{v}_{A,B}^\wedge & {}^B\boldsymbol{\omega}_{A,B}^\wedge \end{bmatrix} \in \mathbb{R}^{6\times6}. \tag{5} $$

Without loss of generality, we will assume that the inertial frame of reference A is attached to the robot's base with its z-axis parallel to the gravity vector and directed upwards. Frame B is located at the package's *center of mass* (CoM) while frame Q lies on the package surface at the contact point with the suction cup's lip. For simplicity one can assume that frames S and Q are coincident (${}^A\mathbf{H}_Q = {}^A\mathbf{H}_S$) when contact between the suction cup and package is established, and that frames S and B to have the same orientation ${}^A\mathbf{R}_S = {}^A\mathbf{R}_B$. Frame E is placed at the end-point of the tool-arm (which is coincident with the suction cup's fitting) and S at the center of the suction-cup lip's plane, see Fig. 2. For further details on the used notation, the reader is referred to [23].

B. Free body diagram

In order to determine the different forces acting on the system, we will make use of the following **modeling assumptions**:

(i) there is no slippage between the held package and the suction-cup lip,
(ii) the suction cup's mass can be neglected in comparison to the held package and tool-arm,
(iii) the inner-pressure within the suction cup is constant.

The deformation of the suction cup's bellow is mainly due to the gravitational and inertial forces of the held package and its mass is negligible with respect to both the package and the tool-arm. Furthermore, since we are interested in modeling the suction cup's behavior during holding phase, we are assuming a rigid connection between the held package and the suction-cup lip, such that there is no relative motion between them nor the need to model frictional effects. Moreover, while the elastic characteristics of the suction cup change when changing the internal pressure, as shown in [26], maintaining the internal pressure at a constant value is a legitimate assumption since in real-world applications the pressure is not susceptible to change.

A free body diagram with the different wrenches between the interconnected parts of the *tool-arm* + *Suction cup* + *Package* system is shown in Fig. 2. The wrench acting from the tool-arm on the suction cup expressed in frame E is denoted by ${}_E\mathbf{f}_{TA\to SC}$ while ${}_S\mathbf{f}_{PA\to SC}$ is the wrench acting from the package on the suction cup in frame S. According to Newton's third law,

$$ {}_E\mathbf{f}_{TA\to SC} = -{}_E\mathbf{f}_{SC\to TA} \quad \text{and} \quad {}_S\mathbf{f}_{PA\to SC} = -{}_S\mathbf{f}_{SC\to PA}, $$

and, due to assumption **(ii)**, one can also state that

$$ {}_E\mathbf{f}_{TA\to SC} = -{}_E\mathbf{f}_{PA\to SC} \quad \text{or} \quad {}_S\mathbf{f}_{TA\to SC} = -{}_S\mathbf{f}_{PA\to SC}, $$

with clear meaning of the symbols. Finally, ${}_B\mathbf{f}_g$ is the gravitational wrench acting at the CoM expressed in frame B.

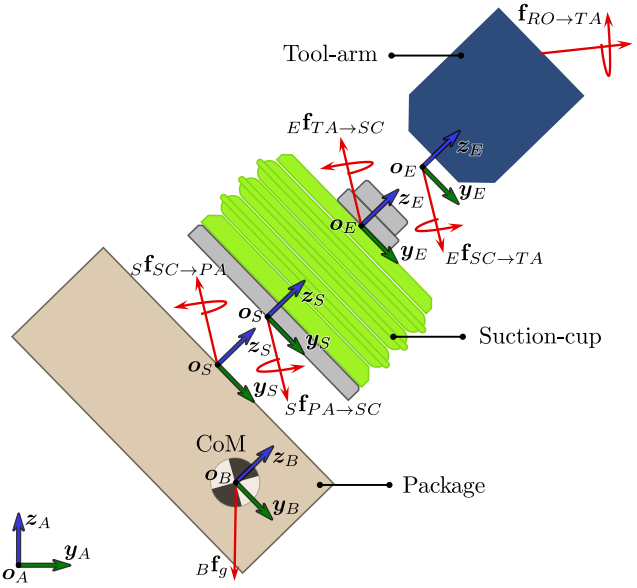

Fig. 2: Free Body Diagram of the bellows suction cup and package in a planar perspective. In the picture, ${}_B\mathbf{f}_g$ is the gravitational wrench acting on the center of mass frame of the package. ${}_S\mathbf{f}_{SC\to PA}$ is the wrench acting on the package applied by the suction cup, and similarly for the other expressions.

C. Coupled package-suction cup system

As already mentioned, we model the bellows suction cup and the package as a driven mass-spring-damper system. The left side of Fig. 3, shows the nominal configuration of the suction cup, corresponding to holding an ideal massless plate. Given the definition of frames S and E, we have

$$ {}^E\mathbf{H}_S = \begin{bmatrix} \mathbf{I} & -l_0{}^E\boldsymbol{z}_E \\ \mathbf{0}_{3\times1} & 1 \end{bmatrix}, \tag{6} $$

with l_0 being the distance between E and S along the z-axis, and ${}^E\boldsymbol{z}_E = [0;0;1]$ where ";" denotes row concatenation. $\mathbf{I} \in \mathbb{R}^{3\times3}$ is the 3×3 identity matrix, if not otherwise specified with a subscript, and $\mathbf{0}_{3\times1}$ is the null matrix of dimension 3×1. Due to this choice of the nominal configuration and assumption (iii), we are essentially modeling the composite behavior of the suction-cup's material and vacuum as a single visco-elastic element, i.e., the 6D linear-torsional spring and damper. Therefore, the wrench acting on the package applied by the suction cup can be modeled as the spring and damper effects of the suction cup's bellow as

$$ \begin{aligned} {}_S\mathbf{f}_{SC\to PA} = {}_S(\mathbf{f}_{SPRG})_{SC\to PA}({}^E\mathbf{H}_S;\mathbf{K}) \\ + {}_S(\mathbf{f}_{DAMP})_{SC\to PA}({}^E\mathbf{H}_S;{}^S\mathbf{v}_{E,S};\mathbf{D}) \end{aligned} \tag{7} $$

with $\mathbf{K},\mathbf{D} \in \mathbb{R}^{6\times6}$ the symmetric and positive (semi-)definite stiffness and damping matrices, respectively, and ${}^S\mathbf{v}_{E,S}$ the twist between frames E and S.

Following [21] we introduce two frames, S_1 and S_2 to parameterize the suction cup deformation (see right side of Fig. 3). These two frames S_1 and S_2 coincides at the rest pose. Frame

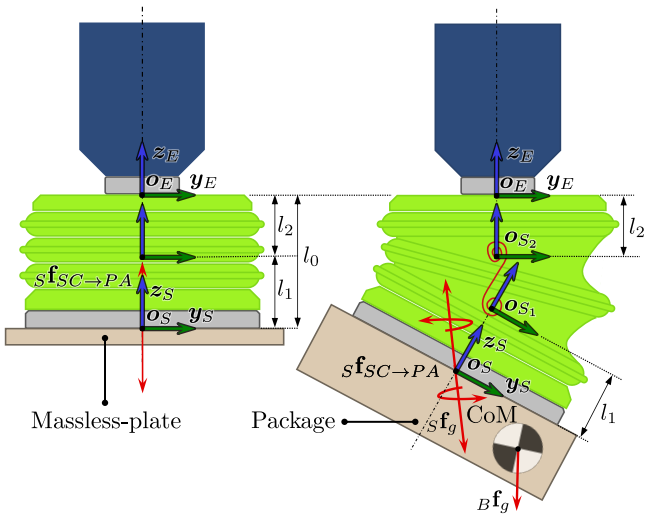

Fig. 3: Schematic representation of the bellow suction cup. (Left) The nominal configuration of the suction cup: the bellows are compressed due to the internal pressure while holding an ideal massless plate. (Right) A package is held by the vacuum suction force while the gravitational force elongates the bellows. The frames for relative displacement S_1 and S_2 are also drawn.

S_1 is rigidly connected to frame S and has the same orientation, similarly for frame S_2 with frame E. Such frames represent the centers of compliance and define the relative displacement between bodies L_1 and L_2. L_1, is the held object together with the part of the bellows suction cup between frames S_1 and S while L_2 denotes the rigid body composed by the tool-arm, including the part of the bellows suction cup between frames S_2 and E. We assume this two frames to be linked to each other via a coupled linear-torsional 6D spring and damper. Straightforwardly, we have

$$ {}^{S_2}\mathbf{H}_{S_1} = {}^{S_2}\mathbf{H}_E\, {}^{A}\mathbf{H}_E^{-1}\, {}^{A}\mathbf{H}_S\, {}^{S}\mathbf{H}_{S_1}. \tag{8} $$

The remaining constant terms in (8) are given by

$$ {}^{S_2}\mathbf{H}_E = \begin{bmatrix} \mathbf{I} & l_2\, {}^{E}\boldsymbol{z}_E \\ \mathbf{0}_{3\times 1} & 1 \end{bmatrix}, \; {}^{S}\mathbf{H}_{S_1} = \begin{bmatrix} \mathbf{I} & l_1\, {}^{S}\boldsymbol{z}_S \\ \mathbf{0}_{3\times 1} & 1 \end{bmatrix} \tag{9} $$

where l_1 and l_2 are fixed link lengths (cf. Fig. 3). From (8) and (9), we get

$$ {}^{S_2}\mathbf{H}_{S_1} = \left[\begin{array}{c|c} {}^{E}\mathbf{R}_S & l_2\, {}^{E}\boldsymbol{z}_E + l_1\, {}^{E}\mathbf{R}_S\, {}^{S}\boldsymbol{z}_S + {}^{E}\mathbf{o}_S \\ \hline \mathbf{0}_{3\times 1} & 1 \end{array}\right]. \tag{10} $$

D. Held-package dynamics

When holding a rigid package of known inertia, its dynamics can be described by the well known Newton-Euler equation of motion

$$ {}_B\mathbb{M}_B\, {}^{B}\dot{\mathbf{v}}_{A,B} + {}^{B}\mathbf{v}_{A,B}\, \bar{\times}^{*}\, {}_B\mathbb{M}_B\, {}^{B}\mathbf{v}_{A,B} = {}_B\mathbf{X}^{S}\, {}_S\mathbf{f}_{SC\to PA} + {}_B\mathbf{f}_g, \tag{11} $$

where ${}_B\mathbb{M}_B$ is the package's generalized inertia matrix

$$ {}_B\mathbb{M}_B = \begin{bmatrix} m\mathbf{I} & \mathbf{0}_{3\times 3} \\ \mathbf{0}_{3\times 3} & {}_B\mathbb{I}_B \end{bmatrix} \in \mathbb{R}^{6\times 6}, \tag{12} $$

with $m \in \mathbb{R}$ its mass and ${}_B\mathbb{I}_B \in \mathbb{R}^{3\times 3}$ the symmetric inertia tensor expressed in frame B. The term ${}_B\mathbf{X}^{S}\, {}_S\mathbf{f}_{SC\to PA}$, is the suction cup force (7) reported to the CoM frame B and

$$ {}_B\mathbf{f}_g = {}_B\mathbf{X}^{B[A]}\, {}_{B[A]}\mathbf{f}_g = \underbrace{\begin{bmatrix} {}^{B}\mathbf{R}_A & \mathbf{0}_{3\times 3} \\ \mathbf{0}_{3\times 3} & {}^{B}\mathbf{R}_A \end{bmatrix}}_{{}_B\mathbf{X}^{B[A]}} \begin{bmatrix} 0 \\ 0 \\ -mg \\ 0 \\ 0 \\ 0 \end{bmatrix} \tag{13} $$

is the gravitational wrench, where $g = 9.81[m/s^2]$ is the gravitational acceleration.
In the next section, we detail the 6D suction cup spring wrench model.

III. Spring Wrench Modeling

As mentioned in Section II, the coupled suction cup and held object is modeled as a driven spatial mass-spring-damper system. Inspired by the two-part work of Fasse [21], [27], we propose a novel geometric potential energy function defined on all SE(3). Unlike for [27], our spring wrench expression in exponential coordinates is derived from our proposed geometric potential energy function, allowing for large deformations and ensuring that the spring wrench is conservative and has geometric meaning. The proposed potential energy has the following expression

$$ P_0(\mathbf{H}) = \frac{1}{8}\begin{bmatrix} (\mathbf{I}+\mathbf{R}^\top)\mathbf{o} \\ (\mathbf{R}-\mathbf{R}^\top)^\vee \end{bmatrix}^\top \mathbf{K} \begin{bmatrix} (\mathbf{I}+\mathbf{R}^\top)\mathbf{o} \\ (\mathbf{R}-\mathbf{R}^\top)^\vee \end{bmatrix}, \tag{14} $$

where, for the sake of brevity, we use $\mathbf{H} = (\mathbf{R}, \mathbf{o})$ to indicate the local deformation ${}^{S_2}\mathbf{H}_{S_1} = ({}^{S_2}\mathbf{R}_{S_1}, {}^{S_2}\mathbf{o}_{S_1})$ appearing in (10) and

$$ \mathbf{K} = \begin{bmatrix} \mathbf{K}_t & \mathbf{K}_c \\ \mathbf{K}_c^\top & \mathbf{K}_o \end{bmatrix} \in \mathbb{R}^{6\times 6} \tag{15} $$

is a symmetric positive definite matrix. The potential energy (14) is a quadratic form with respect the local deformation

$$ \frac{1}{2}\begin{bmatrix} (\mathbf{I}+\mathbf{R}^\top)\mathbf{o} \\ (\mathbf{R}-\mathbf{R}^\top)^\vee \end{bmatrix}, \tag{16} $$

where $1/2\,(\mathbf{R}-\mathbf{R}^\top)$ is the well-known computationally efficient approximation of $\log(\mathbf{R})$ (see Appendix A) and $1/2\,(\mathbf{I}+\mathbf{R}^\top)\mathbf{o}$ is a regularized deformation vector, similar to the term appearing in the spring wrench proposed by [27, Section 2.2], that ensures the port-invariant property $P_0(\mathbf{H}) = P_0(\mathbf{H}^{-1})$. Further details on the derivation, novelty, and properties of the chosen potential function are provided in Appendix A. The local deformation (16) also ensures that the matrix $\mathbf{K}$ can be interpreted as a classical stiffness matrix for small deformations ($\mathbf{R} \approx \mathbf{I}$ and $\mathbf{o} \approx \mathbf{0}$). In (14), the symmetric matrices $\mathbf{K}_t$, $\mathbf{K}_o \in \mathbb{R}^{3\times 3}$ represent the translational and rotational stiffness terms, while $\mathbf{K}_c \in \mathbb{R}^{3\times 3}$ represent the coupling term.

Straightforward geometric differentiation of the potential energy (14) with respect to the displacement $\mathbf{H}$ (cf. Appendix A for the details) results in

$$ {}_{S_1}(\mathbf{f}_{SPRG})_{L_2\to L_1}(\mathbf{H}) = \\ -\frac{1}{4}\begin{bmatrix}\mathbf{R}^\top+\mathbf{I} & \mathbf{0}_{3\times3}\\ -(\mathbf{R}^\top\mathbf{o})^\wedge & (tr(\mathbf{R})\mathbf{I}-\mathbf{R})\end{bmatrix}\mathbf{K}\begin{bmatrix}(\mathbf{R}^\top+\mathbf{I})\mathbf{o}\\ (\mathbf{R}-\mathbf{R}^\top)^\vee\end{bmatrix}. \quad (17)$$

This is the wrench applied by body L_2 via the spring to body L_1, expressed in the coordinates of frame S_1. The spring wrench (17) can be written with respect to the suction cup frame S and be then used in (7) and (11) via

$$ {}_S(\mathbf{f}_{SPRG})_{SC\to PA} = {}_S\mathbf{X}^{S_1}\,{}_{S_1}(\mathbf{f}_{SPRG})_{L_2\to L_1}. \quad (18)$$

A. Exploiting symmetries for model parameter reduction

Any attempt at estimating the stiffness matrix $\mathbf{K}$ appearing in (15) will require the estimation of $6(6+1)/2 = 21$ parameters. Identifying the 21 has led us, in practice, to completely unreliable results. However, the family of suction-cups we are considering (see Fig. 4) clearly exhibits a continuous axial symmetry and, as it will be better clarified in the following, has a decoupling between torsional and bending stiffness in rotation direction orthogonal to the axis of symmetry. These two facts leads to the key result that only 5 parameters instead of 21 are actually needed. This greatly simplifies the parameter identification and data collection procedure, still characterizing the 6D elastic behavior of the suction-cup's bellows using a lumped model such as (17).

*1) **Axial symmetry**:* A continuous axial symmetry for a 6D spring model corresponds to the invariance of the spring potential such as $P_0(\mathbf{H})$ in (14) with respect to the mounting angle. Mathematically, this constraint is written as

$$ P_0(\mathbf{H}) = P_0(\mathbf{T}_\theta^{-1}\mathbf{H}\mathbf{T}_\theta) \quad (19)$$

for any arbitrary spring deflection $\mathbf{H} = {}^{S_2}\mathbf{H}_{S_1} \in \mathrm{SE}(3)$ and spring mounting rotations $\theta \in [0, 2\pi)$. In (19),

$$ \mathbf{T}_\theta := \begin{bmatrix}\mathbf{R}_z(\theta) & \mathbf{0}_{3\times1}\\ \mathbf{0}_{1\times3} & 1\end{bmatrix} \in \mathrm{SE}(3) \quad (20)$$

denotes a rigid transformation expressing a pure rotation of θ radians about the spring axis, with $\mathbf{R}_z$ denoting the standard rotation matrix about the z axis, which is the axis of symmetry of the spring (cf. the frames S_1 and S_2 defined in Section II). Assuming (19), we obtain the following result.

Proposition 1. *If the spring potential* (14) *satisfies the invariance property* (19)*, then the symmetric stiffness matrix* $\mathbf{K}$ *appearing in* (14)*, and as a consequence in spring wrench* (17)*, has the following structure*

$$ \mathbf{K} = \left[\begin{array}{ccc|ccc} k_{t_{xx}} & 0 & 0 & k_{c_{xx}} & k_{c_{xy}} & 0\\ 0 & k_{t_{xx}} & 0 & -k_{c_{xy}} & k_{c_{xx}} & 0\\ 0 & 0 & k_{t_{zz}} & 0 & 0 & k_{c_{zz}}\\ \hline k_{c_{xx}} & -k_{c_{xy}} & 0 & k_{o_{xx}} & 0 & 0\\ k_{c_{xy}} & k_{c_{xx}} & 0 & 0 & k_{o_{xx}} & 0\\ 0 & 0 & k_{c_{zz}} & 0 & 0 & k_{o_{zz}} \end{array}\right], \quad (21)$$

with just 7 independent parameters $k_{t_{xx}}$, $k_{t_{zz}}$, $k_{c_{xx}}$, $k_{c_{zz}}$, $k_{c_{xy}}$, $k_{o_{xx}}$, *and* $k_{o_{zz}} \in \mathbb{R}$.

Proof. See Appendix B.

A further reduction from 7 to 5 parameters is possible, as we explain in the following.

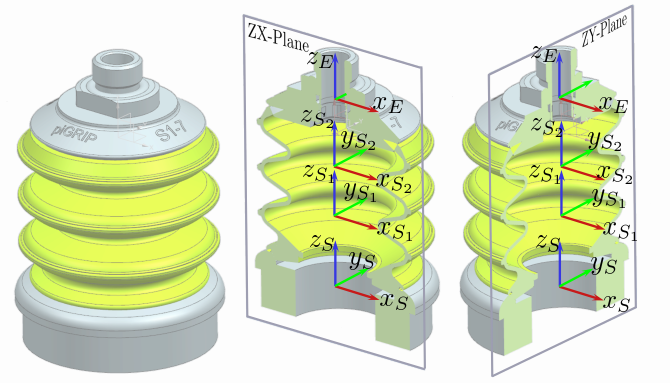

Fig. 4: CAD model of the Suction cup with its cross-sections on the ZX- and ZY-planes to highlight its axial symmetry.

*2) **In-plane twist-wrench relationship**:* If, besides having a continuous axial symmetry, the suction cup also has a mirror symmetry on any plane that contains the axis of symmetry, then one expects that deforming the suction cup in that plane will lead to a resulting in-place forces and a resulting torque that is orthogonal to it. This is also confirmed by physical experiments: tilting the tool-arm while carrying a payload whose CoM is lying along the symmetry axis, leads to a bending of the suction cup within the plane containing the gravity direction and tool-arm axis, with no lateral deviation or suction cup twisting. This behavior clearly suggests that the coupling terms in the stiffness matrix (21) that induce out-of-plane forces and in-plane torques must be zero.

Proposition 2. *If the spring potential* (14) *satisfies both the invariance property* (19) *and has a mirror symmetry, i.e., the translation happens in a plane which contains the axis of symmetry and that the rotation being orthogonal to that plane generate forces only in the same plane and a torque only along the same axis , then the coupling stiffness matrix* $\mathbf{K}_c$ *appearing in* (15) *has zero elements on the diagonal and thus the symmetric stiffness matrix* $\mathbf{K}$ (21) *is reduced to*

$$ \mathbf{K} = \left[\begin{array}{ccc|ccc} k_{t_{xx}} & 0 & 0 & 0 & k_{c_{xy}} & 0\\ 0 & k_{t_{xx}} & 0 & -k_{c_{xy}} & 0 & 0\\ 0 & 0 & k_{t_{zz}} & 0 & 0 & 0\\ \hline 0 & -k_{c_{xy}} & 0 & k_{o_{xx}} & 0 & 0\\ k_{c_{xy}} & 0 & 0 & 0 & k_{o_{xx}} & 0\\ 0 & 0 & 0 & 0 & 0 & k_{o_{zz}} \end{array}\right] \quad (22)$$

with just 5 independent parameters $k_{t_{xx}}$, $k_{t_{zz}}$, $k_{c_{xx}}$, $k_{c_{zz}}$, $k_{c_{xy}}$, $k_{o_{xx}}$, *and* $k_{o_{zz}} \in \mathbb{R}$.

Proof. See Appendix C.

These results not only lead to an easier identification problem as we shows in the following section, but significantly reduces also the experimental effort required to collect the data needed to build the optimization problem (cf. Section V).

IV. Parameter identification

In Sections II and III, we provided a parameterized model to predict the wrench acting on the suction cup lip frame S based on its relative displacement with respect to the tool-arm end frame E. Despite dynamic model parameters (stiffness and

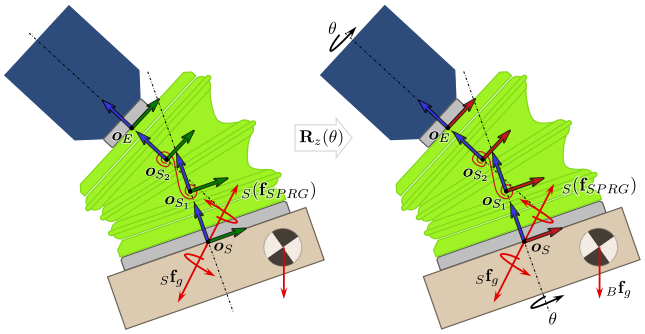

Fig. 5: Representation of the equivariance notion of the spring wrench. The configuration dependent spring wrench in a certain pose (left) and after a rotation of the suction cup of $\theta = 90°$ about the symmetry axis (right). Notice how the frames E, S_2, S_1 and S results to be rotated of $90°$ about their z-axes. Despite the rotation, the package and the tool arm experience the same contact wrench before and after the suction cup's rotation.

damping) can be identified simultaneously, we opted for a two-step identification procedure in which we firstly identify the stiffness from static experiments. Here, we then introduce the *parameter identification* problem that will identify the entries of the stiffness matrix $\mathbf{K}$.

In static conditions, the left hand side of (11) corresponding to inertial forces are clearly zero and we obtain the force balance

$$-{}_B\mathbf{X}^S\,{}_S\mathbf{X}^{S_1}\,{}_{S_1}(\mathbf{f}_{SPRG})_{L_2\to L_1} = {}_B\mathbf{f}_g \tag{23}$$

or equivalently

$$-{}_{S_1}(\mathbf{f}_{SPRG})_{L_2\to L_1} = {}_{S_1}\mathbf{X}^B\,{}_B\mathbf{f}_g = {}_{S_1}\mathbf{f}_g. \tag{24}$$

Assuming to know the held package inertial properties, its CoM location with respect to the lip frame (${}^S\mathbf{H}_B$), and the suction cup center of compliance parameterized by l_1 in (9), we can compute the right hand side of (24). On the other hand, the spring wrench in (24), whose expression is provided in (17), depends linearly on the elements of $\mathbf{K}$ that can be rearranged in a vector $\bar{\boldsymbol{k}} = [k_1; \ldots; k_n]$, allowing to write the system for each static configuration $\mathbf{H}^i$ and sample ${}_{S_1}\mathbf{f}_{g_i}$ as

$$\boldsymbol{A}(\mathbf{H}^i)\bar{\boldsymbol{k}} = {}_{S_1}\mathbf{f}_{g_i}, \tag{25}$$

for $i \in \{1, \ldots, N\}$. In (25), $\boldsymbol{A}(\mathbf{H}^i) \in \mathbb{R}^{6\times n}$, is the known configuration dependent regressor matrix. By staking various instances of (25) for different measurements, one has that

$$\bar{\boldsymbol{A}}\bar{\boldsymbol{k}} = \begin{bmatrix} \boldsymbol{A}(\mathbf{H}^1) \\ \vdots \\ \boldsymbol{A}(\mathbf{H}^N) \end{bmatrix} \bar{\boldsymbol{k}} = \begin{bmatrix} {}_{S_1}\mathbf{f}_{g_1} \\ \vdots \\ {}_{S_1}\mathbf{f}_{g_N} \end{bmatrix} = {}_{S_1}\bar{\mathbf{f}}_g, \tag{26}$$

with $\bar{\boldsymbol{A}} \in \mathbb{R}^{6N\times n}$ and ${}_{S_1}\bar{\mathbf{f}}_g \in \mathbb{R}^{6N\times 1}$. To identify the stiffness parameters, one can solve an ordinary least-squares (LS) problem

$$\bar{\boldsymbol{k}}^* = \arg\min_{\bar{\boldsymbol{k}}} \left\| \sum_{i=1}^{N} w_i(\boldsymbol{A}(\mathbf{H}^i)\bar{\boldsymbol{k}} - {}_{S_1}\mathbf{f}_{g_i}) \right\|^2 \tag{27}$$

where $w_i \in \mathbb{R}$ is a weighting factor, or equivalently via pseudo-inversion

$$\bar{\boldsymbol{k}} = \bar{\boldsymbol{A}}^+\,{}_{S_1}\bar{\mathbf{f}}_g \tag{28}$$

where $\bar{\boldsymbol{A}}^+ = (\bar{\boldsymbol{A}}^\top \boldsymbol{W} \bar{\boldsymbol{A}})^{-1}\bar{\boldsymbol{A}}^\top \boldsymbol{W}$ denotes the left Moore-Penrose weighted pseudo-inverse with weighting matrix $\boldsymbol{W} = diag(w_1\mathbf{I}_6, \ldots, w_N\mathbf{I}_6)$.

V. Experimental results

In order to solve the optimization problem (27) and identify the stiffness parameters of the spring wrench model, we need to know the suction cup's configuration, *i.e.*, the relative pose between the suction cup's fitting and lip, as well as the wrench acting on the lip. To this end, an OptiTrack system composed of 6 cameras (four Prime 17W and two Prime x22) operating at 360 Hz with sub-millimeter accuracy is used to track the passive markers placed on the *fitting collar* and the held object. As held object we use a custom designed *Variable-Inertia-Object* (VIO), as shown in Fig. 6a. It consist of the top plate equipped with passive markers, seven racks with an internal 7×7 grid that can hold metal spheres, and the lip-holders on top of the plate to constrain the suction cup's lip. The number and configuration of the spheres in the racks determines the total VIO's mass, CoM location and the principal axes of the inertia tensor. By tracking its top-plate with the OptiTrack, we can estimate the wrench applied by the VIO acting at the center of the lip-plate interface area. Since our goal is to capture only the bellow's behaviour, we have constrained the suction cup's lip to the VIO plate for experimental repeatability, to guarantee that the center of the lip is coincident with the plate's center, to prevent potential slippage and detachment of the suction-cup lip from the package.

A custom-designed vacuum gripper, equipped with a Venturi ejector for creating the vacuum and operating at an inlet pressure of 3.7 [bar], is mounted on a tool-changer at the UR10's flange. It uses a Schmalz VS-VP8-SA-M8-4 [28] pressure sensor to monitor the inner-pressure ($\sim$ 0.49 Volts – we report the sensor reading because the pressure-voltage characteristic of the sensor reported its datasheet is wrong) at the attached Piab's piGRIP S1-7 suction cup used as end-effector.

The experimental data and MATLAB code developed in this work will be made available at https://gitlab.tue.nl/robotics-lab-public/suction cup-modeling/.

A. Data collection

A total of 1200 static poses were recorded in 6 distinct sessions with varying inertial parameters of the payload, as indicated in Table I.

TABLE I: Experiment payload parameters.

	Sess. 1	Sess. 2	Sess. 3	Sess. 4	Sess. 5	Sess. 6	unit
# Exps	245	242	162	247	288	16	-
mass	1.948	2.366	1.421	1.014	2.821	1.747	kg
$({}^S\mathbf{o}_B)_x$	0	0	0	-24.3	-30.55	0	mm
$({}^S\mathbf{o}_B)_y$	0	0	0	-24.3	30.55	0	mm
$({}^S\mathbf{o}_B)_z$	-81.37	-79.03	-55.22	-27.83	-75.95	-80.57	mm

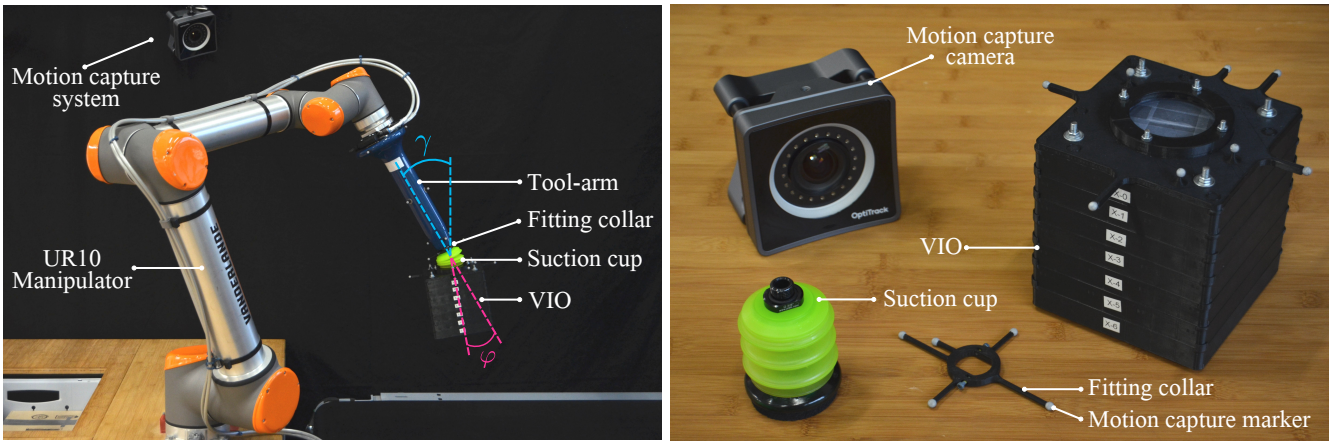

(a) (b)

Fig. 6: Experimental setup used for collecting the data. Full setup with the different components indicated (a), and detailed picture showing, in particular, the motion capture camera, the Fitting Collar for tracking the suction cup's attachment, the Piab's piGRIP S1-7 suction cup, and the Variable Inertia Object VIO (b). The tool-arm, suction cup's fitting and the package's frame (VIO's top plate) are equipped with reflective passive markers used for tracking their pose with the OptiTrack system, also indicated in Fig. 6b. In Fig. 6a, γ is the tilting angle between the tool-arm and the vertical axis while φ is the tilting angle between the fitting and the lip (suction cup's bending angle).

For each of the six experimental sessions, some or all of the VIO's racks were loaded with a number of metal spheres weighing 32.6 grams each. Each rack weights 81 grams while the VIO plate 101 grams. Once the VIO is assembled and the suction-cup's lip attached to the plate by mean of the lip-holders, the coupled system *VIO + suction cup* is mounted on the tool-arm of the vacuum gripper. At this stage, vacuum is activated and the robot is commanded to adopt a given configuration. After 5 seconds, a recording script is launched that records the robot's log, among which the pressure sensor signal, and triggers the OptiTrack recording for 3 seconds. These periods were empirically found as a sufficient amount of time for the motion of the held package to damp out and for the recording to filter out any remaining oscillation around the equilibrium. Then, a new robot configuration is commanded and the entire recording process repeated. Once a data-collection session is completed, a new VIO configuration is assembled and mounted back on the tool-arm for the next one. Each recorded position and orientation is filtered and averaged to obtain a single SE(3) point. In view of the further expansion of this research to the fully dynamic case, we have employed [29] already for filtering the rotation information. The sessions spanned the tool-arm's inclination ranging from straight vertical ($\gamma = 0°$), to large inclination ($\gamma \approx 65°$ cf. Fig. 6a). The poses of frame S with respect to frame E for the 1200 static experiments can be seen in Fig. 7. Prior to each experimental recording session, a calibration experiment is performed in which, by keeping the tool-arm vertically aligned with the gravity vector, a rotation of 360+ degrees about the symmetry axis is continuously recorded. This data is needed to align the coordinate frames of the assets (rigid body frames) defined in the OptiTrack's software suit *Motive* and their corresponding frames as defined in this paper. The collected data was then split into two subsets, namely the training and the test sets. The Training set contains half of the data points in sessions 1 to 5 having picked one data point each two (592 points). The test set contains the remaining half of the data points in sessions 1 to 5 (592 points) plus the entire session 6 (16 experiments with a different mass and CoM location which is not used in the identification procedure).

B. Nominal length identification

To properly compute the suction-cup's elongation one needs to identify its nominal configuration which, as stated in Section II, given the frames definitions, it only depends on the relative vertical distance l_0 between frames E and S (cf. Fig. 3), which

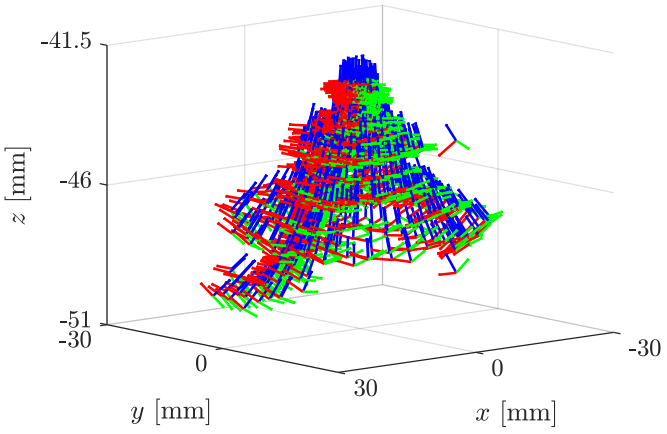

Fig. 7: Experimental data of the relative suction cup pose: the 1200 filtered static poses of frame S with respect to frame E. Note how the lip's deformation distributes itself in a bell-shape fashion. With heavier payload, the frame S gets farther away for the suction cup attachment frame E. The rest position of frame S corresponds to (0,0, $-l_0$) in the plot.

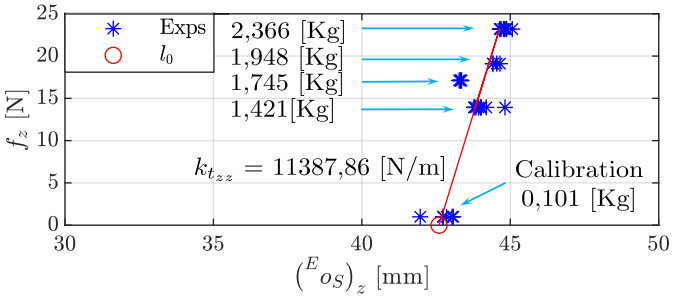

Fig. 8: Nominal length identification: the gravitational vertical force is plotted against the relative Fitting-lip elongation at different payloads when the tool-arm is vertically aligned with the gravity vector. The red line is the linear fitting to this data. The nominal configuration length $l_0 = 42.6\,mm$ is the relative fitting-lip distance at zero gravitational force.

correspond to the pose of the lip when the suction cup is holding an ideal massless plate.

It is possible to estimate the rest pose of the suction-cup's lip with respect to the fitting using calibration recordings and experiments in which the tool-arm is vertically aligned with the gravity vector of those sessions with the payload along the symmetry axis. From the stiffness matrix structure (22), one notes that the linear stiffness along the z-axis is fully decoupled. Assuming linear behaviour close to the nominal configuration, one can fit a line through the data to find l_0. The force-elongation measurements are shown in Fig. 8, together with the nominal length ($l_0 = 42.6\,mm$) estimated via linear fitting and indicated in the plot with a red circle. The slope of the fitted line in Fig. 8 corresponds to the linear stiffness along the z-axis, which resulted to be $k_{t_{zz_0}} = 11387.86$ kg/m, giving us a first estimate of its magnitude near equilibrium. Indeed, as it will be clear in the following subsection, when estimating the stiffness parameters using data up to $\varphi = 5°$, the identified $k_{t_{zz_0}} \sim 11000\,kg/m$.

C. Identification results

The proposed spring wrench model linearly approximate the behavior of the suction cup near the rest position via a stiffness matrix and it is to be expected that for larger deformations this single matrix in combination with the potential energy expression (14) might fail to capture correctly the pose-wrench relationship. From experimental observations we have found that the nonlinear behavior of the suction cup becomes more pronounced the more the relative inclination between the fitting and the lip (φ, in Fig. 6a) becomes prominent, so we will use this angle as weighting criteria for the identification. In our experiments, $\varphi \in (0, 50)\,deg$. With the bin-to-bin robotic application shown in Fig. 1 in mind, in which we envision novel motion primitives for tightly stuffing boxes between each other and where, from preliminary experiments, the relative suction-cup's tilting angle (φ) can reach 20°, we have chosen $w_i = 10\,exp(-0.075\varphi_i)$ as weighting function. With this choice, we optimize the stiffness parameters such that the pose error around $\varphi = 20°$ is minimized (cf. Fig. 9).

*1) **Location of the centers of stiffness**:* Before applying the weighted least-squares method (28), we need to define the location of the *centers of stiffness*, *i.e.*, the location of the frames S_1 and S_2 shown in Fig. 3. According to [21], this two frames must be coincident at equilibrium. Furthermore, from linear stiffness theory [21, Section 4.1] and recalling (15), if the $tr(\mathbf{K}_t)$ is not an eigenvalue of $\mathbf{K}_t$ then, for each body there exist a unique center of stiffness at which $\mathbf{K}_c$ is symmetric. Given the structure of the stiffness matrix (22), unless $k_{t_{xx}} = 0$, $tr(\mathbf{K}_t)$ will never be an eigenvalue of $\mathbf{K}_t$. So, it exist a unique point at which $\mathbf{K}_c$ is symmetric.

Furthermore, given that $\mathbf{K}_c$ in (22) is always skew, asking for $\mathbf{K}_c$ to be also symmetric implies $\mathbf{K}_c$ (equivalently, $k_{c_{xy}}$) to be zero. We found therefore a further reduction of the number of parameters to be fitted in our model. Due to the suction-cup's symmetry, the centers of stiffness should lie along the symmetry axis and we find its location numerically by iterating the least-squares problem over different values of the convex combination parameter α, where α is such that $l_2 = \alpha\, l_0$ and $l_1 = (1-\alpha)\, l_0$.

*2) **Identifiability**:* The spring wrench model is *structurally identifiable* [30] since it linearly depends on all its unknown parameters, hence, it is theoretically possible to identify them all. However, structural identifiability only implies *practical identifiability* for an infinite amount of data with zero noise. Therefore, before starting the identification process, especially for experimental data with large measurement noise, it is advisable to assess the informativeness of the collected data in order to estimate the parameter with adequate accuracy. We note first that the maximum elongation of the suction cup's lip with respect to its nominal rest pose is about ±25 mm along x- and y-axes while it is less than 8 mm along the z-axis (see Fig. 7); OptiTrack's 3D position accuracy is ± 0.2 mm for each rigid body, thus, the noise level is significant for the relative displacements we are measuring. We are concerned about the practical identifiability of the torsional stiffness about the z-axis, since it seems to be quite high compared to the other two axes. Indeed, it is not possible to manually twist the bellows suction cup about the z-axis; This means that in a real application, slippage between the suction-cup's lip and the held object, due to a torque about the z-axis, may happen way before a noticeable torsion of the bellows suction cup is detected. This is an additional reason why we constrained the suction-cup's lip to the VIO top surface. On the other hand, looking into the symbolic expression of the regressor ($\boldsymbol{A}(\mathbf{H})$ in (25)) and knowing the expression of the rotation matrix constructed from the axis/angle representation, parameter $k_{o_{zz}}$ appears always multiplied by $(R_{1,2} - R_{2,1}) = -2u_z sin(\theta)$. Since we are essentially measuring no rotation about the z-axis (even for large off-centered payloads like in Sessions 4 and 5), the data relative to the z component of the axis of rotation is mostly measurement noise, resulting in an arbitrary estimate of the parameter $k_{o_{zz}}$ (cf. Table II).

The identified stiffness parameters at varying α are shown in Table II. The right-most column shows the root-mean-square (RMS) of the residual $\bar{\boldsymbol{r}} = \bar{\boldsymbol{A}}\bar{\boldsymbol{k}} - {}_{S_1}\bar{\mathbf{f}}_g$ for each set of identified parameters, which seems to be insensitive to the location of the centers of stiffness ($\Delta\%_{max} = 0.02\%$). Indeed, the only

TABLE II: 6D identification results at varying α.

α	$k_{t_{xx}}[\frac{N}{m}]$	$k_{t_{zz}}[\frac{N}{m}]$	$k_{o_{xx}}[\frac{Nm}{rad}]$	$k_{o_{zz}}[\frac{Nm}{rad}]$	$k_{c_{xy}}[\frac{N}{rad}]$	**RMS($\bar{r}$)**
0	5126.54	4491.29	4.2487	0.76590	-89.7711	22.122
1/3	5125.12	4491.25	2.6884	0.75320	-16.9759	22.121
0.411093	5124.78	4491.24	2.6218	0.75024	-0.0001	22.120
5/12	5124.76	4491.24	2.6214	0.75003	1.2165	22.120
1/2	5124.39	4491.23	2.6835	0.74686	19.4064	22.120
2/3	5123.66	4491.20	3.1950	0.74052	55.7783	22.120
3/4	5123.30	4491.19	3.6444	0.73736	73.9603	22.120
1	5122.19	4491.13	5.7665	0.72787	128.4904	22.120
3/2	5119.92	4491.00	13.4916	0.70893	237.4773	22.122
2	5117.61	4490.83	25.8524	0.69006	346.3640	22.125
$\Delta\%_{max}$	0.174%	0.01%	886.19%	10.99 %	485.83%	0.02%

values that significantly change are the coupling term $k_{c_{xy}}$ and, proportionally to compensate for the coupling term variation, the bending stiffness $k_{o_{xx}}$, with variations of the 485.83% and 886.19% respectively. The identified value of the torsional stiffness about the z-axis $k_{o_{zz}}$ is, as expected, totally unreliable: although the torsional stiffness of the suction cup is way higher than the bending stiffness, the obtained value is extremely low. Note that fixing the value of $k_{o_{zz}}$ in the range 0 to $10^5\ Nm/rad$ in (27) and then identifying the remaining four parameters, leads to the same results as shown in Table II.

*3) **Performance assessment**:* In order to predict the final rest pose of the modeled *package + suction cup* system, we have numerically implemented the Newton-Euler dynamics (11) in an ODE MATLAB routine, initializing it with the fitting frame's pose from the real experiments and letting the system evolve until the lip settles, pulled by the action of payload's gravitational force. We have assessed the compliance with the principle of total energy conservation of the implemented model by putting zero damping and verifying that the total energy (kinetic + elastic + gravitational) is constant. To generate a steady state, we have added fictitious damping tuned to obtained a critically damped response (damping modeling and parameter identification for the suction cup will be the subject of a future investigation). The pose error is then computed between the predicted and measured rest pose of the lip from each of the 608 experiments of the test set, whose data was not used for the identification. In Fig. 9, the position error ${}^S\mathbf{o}_{\hat{S}}$ and the orientation error ${}^S\mathbf{R}_{\hat{S}}$ and their magnitude corresponding to the pose error ${}^S\mathbf{H}_{\hat{S}} = {}^A\mathbf{H}_S^{-1}{}^A\mathbf{H}_{\hat{S}}$ are plotted as a function of the relative inclination between the fitting and the lip frame φ (using the parameters for α and $\mathbf{K}$ given in the third row of Table II, with $k_{o_{zz}} = 50 Nm/rad$).

The pose error was computed for each set of identified stiffness parameters in Table II at varying α, without finding any significant difference in the predicted rest pose, therefore, Fig. 9 is a good indication of the performance of the model. The first fact to notice is that the system's behaviour can be captured independently of where frames S_1 and S_2 are placed (the maximum deviation of the position and orientation error at varying α is about 0.67 mm and 2.48° respectively) but, when they lie at the center of stiffness, the system further decouples ($k_{c_{xy}} = 0$). The rest position of the suction-cup's lip can be predicted fairly well with the identified parameter, even for quite large deformations: as it can be see from Fig. 9, the pose error remains always below 10 mm and 10°, with a relative

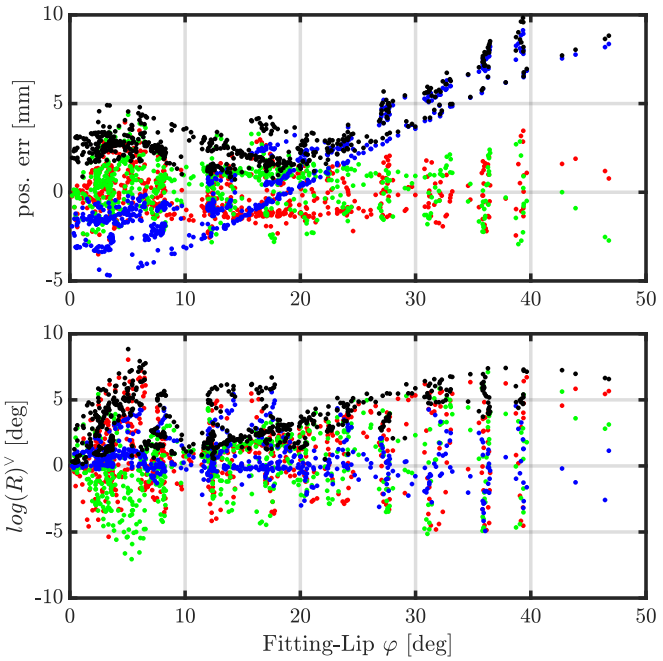

Fig. 9: Rest pose prediction error over relative Fitting-Lip tilt angle φ. (top) $\mathbf{o}_x$(●), $\mathbf{o}_y$(●), $\mathbf{o}_z$(●) and norm $||\mathbf{o}||$(●) of the position error. (Bottom) $\mathbf{u}_x$(●), $\mathbf{u}_y$(●) and $\mathbf{u}_z$(●) components of the rotation vector ($\mathbf{u}$) and its norm ψ(●). The value of the rotational stiffness about z-axis was set to $k_{o_{zz}} = 50\,Nm/rad$ and the center-of-stiffness ratio to $\alpha = 0.411093$.

bending angle that goes up to almost 50°. In Fig. 10, the steady-state of the simulated deformation (black box) against the measured rest pose (red box) for five experiments of the Session 6 are shown. Apart from experiments (d) and (e) for which the position and orientation error (norm $||\mathbf{o}||$ and ψ) reaches 5.4 mm and $\psi = 2,1°$, and 5.1 mm and $\psi = 2,09°$ respectively against a tilt angle of $61,15°$ and $63,18°$ of the tool-arm, which is very unlikely to happen in real logistics applications, the predicted deformations are quite accurate. Furthermore, one can clearly see how the position error along the z-axis increases with the relative fitting-lip tilt angle (Fig. 9 top).

D. Exploiting equivariance to obtain a 2D problem

As discussed in section III-A, if the stiffness matrix presents a certain structure, the spring wrench corresponding to a suction cup that is axially symmetric satisfies the equivariance property for rotations about the axis of symmetry. In this subsection, we will show that thanks to this property, one can reduced the amount of data to collect while still obtaining similar results in terms of prediction capability.

Given any suction cup configuration (${}^{S_2}\mathbf{H}_{S_1}$) and a wrench acting on it (${}_{S_1}\mathbf{f}$), the equivariance property states that if we rotate the suction cup about its symmetry axis (a simultaneous rotation of frames S_1 and S_2 about their respective z-axes, as shown in Fig. 5, the wrench acting on it only experiences a frame transformation, preserving its magnitude and direction, so the system configuration does not change. By exploiting the equivariance transformation, one can project all the collected

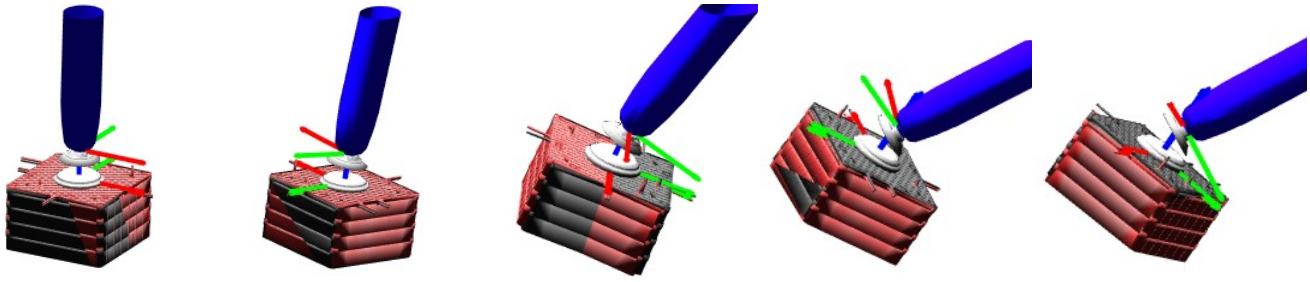

(a) (b) (c) (d) (e)

Fig. 10: Predicted (black) versus measured (red) VIO's rest pose at different tool-arm inclinations. Experiments belongs to Session 6 in Table I, whose data was not used in the identification procedure. The used stiffness values are those in Table II for $\alpha = 0.411093$, setting $k_{o_{zz}} = 50\,Nm/rad$. See Fig. 9 for the complete set of experimental results.

Description	Symbol	a	b	c	d	e	unit
Tool-arm inclination angle w.r.t. the vertical	γ	1,56	12,68	37.26	61,15	63,18	deg
Relative fitting-lip tilt angle	φ	0,58	5,38	12,44	28,03	29.07	deg
Position error norm	$\|\|\mathbf{o}\|\|$	3,1	2.7	1.3	5,1	5.4	mm
Orientation error norm	ψ	0,42	0.77	3.2	2,09	2.1	deg

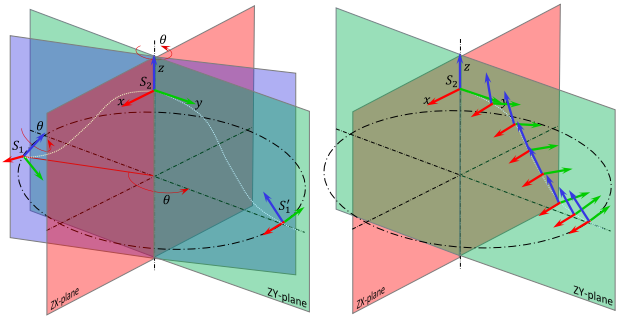

Fig. 11: Equivariance frame transformation: (Left) given a certain spring configuration ($^{S_2}\mathbf{H}_{S_1}$), the rotation angle (θ) needed to bring S_1 to S_1' on the ZY (green) plane by rotating S_1 and S_2 of θ about their z-axes, is the angle between the (blue) plane containing the origins of both frames S_1 and S_2 and the ZY-plane. (Right) The data processed with equivariance lying on one half-plane. Notice the half-bell shape pattern (see Fig. 12 for real data.)

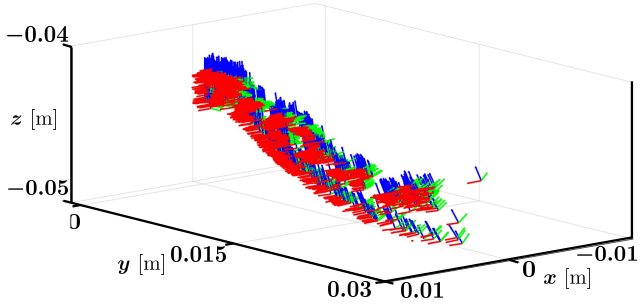

Fig. 12: Data projected with equivariance transformation. Notice that all the frame's origins lie on the ZY-plane alongside their z-axes. Half of the bell-shape is clearly visible as the data is projected on the ZY-plane.

poses into the positive ZY half-plane for instance, by rotating S_1 and S_2 about their respective z-axes of an angle θ, which is the angle between the vertical plane containing the origin of both frames and the ZY plane, as shown in Fig. 11. The whole data-set, visible in Fig. 7, projected with the equivariance transformation can be seen in Fig. 12. Wrenches are transformed accordingly by pre-multiplying them by the wrench transformation matrix (see Appendix B).

TABLE III: 3D identification results at varying α.

α	$k_{t_{xx}}[\frac{N}{m}]$	$k_{t_{zz}}[\frac{N}{m}]$	$k_{o_{xx}}[\frac{Nm}{rad}]$	$k_{c_{xy}}[\frac{N}{rad}]$	**RMS($\bar{r}$)**
0	5929.13	4477.61	4.44	-101.79	30.74
1/3	5996.32	4532.64	2.71	-12.37	30.25
0.411093	5665.86	4506.18	2.60	3.62	30.27
5/12	5670.22	4505.79	2.60	4.97	30.28
1/2	5696.91	4501.40	2.69	25.02	30.38
2/3	5727.35	4497.39	3.33	65.63	30.45
3/4	5744.84	4496.35	3.86	86.21	30.48
1	5758.63	4494.50	6.33	147.63	30.51
3/2	5741.70	4492.84	15.11	269.28	30.52
2	5743.19	4492.00	29.12	391.62	30.54
$\Delta\%_{max}$	5.83 %	1.22 %	1017.4%	484.7%	1.52%

Once the data has been projected on the plane, one can build a reduced optimization problem that takes into account only the entries on such plane, *i.e.*, only the forces along y- and z-axis and the torque about x-axis. Then, optimizing for the (four) non zero components of the sub-stiffness matrix (50) (highlighted in gray in Appendix C) we obtained the parameters reported in Table III at varying of α.

The identified values for the data treated with the equivariance transformation, are comparable with those previously obtained, which in essence captures the same suction cup's behavior. Indeed, the differences in the predicted suction cup lip's rest pose is negligible when using either the values in Table II or Table III.

In this section, we have shown that by only using data lying on one half-plane is sufficient to identify the stiffness parameters. The identified values are comparable with those obtained with the 6D identification procedure, for which the data spans as much as possible the configuration space. This results show that it is possible to identify the parameters of symmetric suction cups with a simpler data-collection procedure that only spans a subspace of the suction-cup's configuration space while being rich enough to practically identify the parameter.

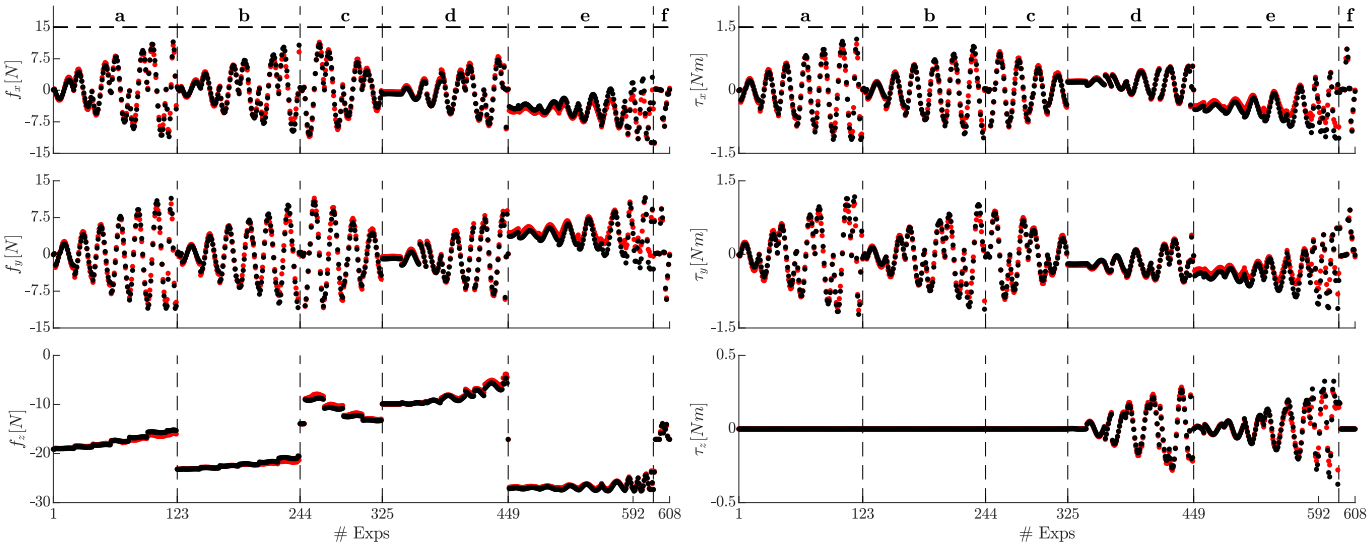

Fig. 13: Predicted (●) and ground-truth (●) wrench comparison for all the 608 experiments in the test set. The letters from **a** to **f** indicates that the data belong to each of the 6 data sessions from 1 to 6 (see Table I). It is possible to appreciate how accurate is the wrench predicted by the proposed model and identification procedure. The RMS error of the predicted and ground-truth forces and torques over the 608 experiments in the test set are: $RMS_f = 0.6949\,N$ and $RMS_\tau = 0.0674\,Nm$.

VI. Conclusions and Future Work

In this paper, we have proposed a 6D elastic model that describes the interaction between the suction cup and suction-held object as a *mass-spring-damper* system. From a newly proposed geometric potential energy function, inspired by classical works but defined in terms of homogeneous transformation matrices, we have derived an energy preserving spring wrench model that linearly depends on the stiffness parameters. We have then delved into the properties of such spring wrench model for axial-symmetric suction cups. These studies have made it possible to better understand the behavior of the suction cups under load and to identify a structure in the stiffness matrix with a consequent significant reduction in the number of parameters to be identified, from 21 to only 5 (or even 4, if the frames that defines the relative deformation are placed at the centers of stiffness). Furthermore, we demonstrate how this simplification translates into a considerably simpler data collection procedure, in which the configuration space to be explored is restricted to a plane by showing that the identification procedure for the planar case with 3 degrees of freedom leads to the comparable results as for the 6D case.

The obtained results in terms of lip pose estimation accuracy are satisfactory for the targeted application, especially if we consider that the data used to fit the stiffness presents large deformations, well beyond the range of intended use. The pose prediction error over the entire test set (608 poses) shows that the position error increases together with the relative fitting-lip angle, being the position error along the z-axis the main source of error. This direction presents indeed the strongest non-linear behaviour, rapidly becoming compliant (less stiff) as the tilting angle increases.

On the other hand, due to the particular choice of the residual in the optimization problem to fit the stiffness parameters, we optimize $\mathbf{K}$ such as to minimize the wrench prediction error. As can be seen from Fig. 13, the predicted wrench results to be quite accurate, with a medium/low signal-to-noise ratio (in particular in the axial translation and the axial rotation).

It is fair to mention that the identified parameters are valid just for a given fixed internal vacuum pressure of the suction cup. Since vacuum grippers are usually equipped with pressure sensor, an easy way to overcome this limitation would be to identify a set of pressure-dependent stiffness parameters. This procedure would not take much effort, as we demonstrate in this work that a simpler data collection procedure can be put in place and the equivariance transformation can be used to augment the data (data-augmentation) by transporting the experiments on the other half-plane, imposing symmetry in the collected data.

The results of this research is potentially valuable for all robotics applications requiring a reliable 6D wrench model of a suction cup in the holding phase for planning, learning, estimation, and control purposes given the wide range of applications involving suction cups, particularly in the field of robotic processes automation in logistics, where suction cups are massively adopted.

In a future publication, we will detail the derivation of a compact viscous model based on similar equivariance principles, that will enable tackling dynamic manipulation problems.

Appendix A
Spring Potential Energy and Wrench Derivation

A. The spring potential energy function

The simplest and intuitive geometric potential energy function one can think of for a 6D spring has the following expression

$$P(\mathbf{H}) = \frac{1}{2}\begin{bmatrix}\mathbf{o}\\ \log(\mathbf{R})^\vee\end{bmatrix}^\top \mathbf{K}\begin{bmatrix}\mathbf{o}\\ \log(\mathbf{R})^\vee\end{bmatrix}. \tag{29}$$

It is easy to verify that this potential is however not port-indifferent, *i.e.*, $P_0(\mathbf{H}) \neq P_0(\mathbf{H}^{-1})$. Indeed, for a given configuration $\mathbf{H}$, the potential energy of $\mathbf{H}^{-1}$ is

$$P(\mathbf{H}^{-1}) = \frac{1}{2}\begin{bmatrix}\mathbf{R}^\top\mathbf{o}\\ \log(\mathbf{R})^\vee\end{bmatrix}^\top \mathbf{K}\begin{bmatrix}\mathbf{R}^\top\mathbf{o}\\ \log(\mathbf{R})^\vee\end{bmatrix}. \tag{30}$$

However, we can easily obtain a port-indifferent potential by construction simply averaging (29) and (30), resulting in

$$\tilde{P}(\mathbf{H}) = \frac{1}{2}(P_0(\mathbf{H}) + P_0(\mathbf{H}^{-1})) = \\ = \frac{1}{4}\left(\begin{bmatrix}\mathbf{o}\\ \log(\mathbf{R})^\vee\end{bmatrix}^\top \mathbf{K}\begin{bmatrix}\mathbf{o}\\ \log(\mathbf{R})^\vee\end{bmatrix} + \begin{bmatrix}\mathbf{R}^\top\mathbf{o}\\ \log(\mathbf{R})^\vee\end{bmatrix}^\top \mathbf{K}\begin{bmatrix}\mathbf{R}^\top\mathbf{o}\\ \log(\mathbf{R})^\vee\end{bmatrix}\right) \tag{31}$$

despite not having the simple structure of a quadratic form.
An alternative, inspired by the average above and reminding the approach in [21], is to use

$$\tilde{P}_0(\mathbf{H}) = \frac{1}{2}\begin{bmatrix}\frac{1}{2}(\mathbf{I}+\mathbf{R}^\top)\mathbf{o}\\ \log(\mathbf{R})^\vee\end{bmatrix}^\top \mathbf{K}\begin{bmatrix}\frac{1}{2}(\mathbf{I}+\mathbf{R}^\top)\mathbf{o}\\ \log(\mathbf{R})^\vee\end{bmatrix}. \tag{32}$$

which is a now quadratic form. Expression (32) can be further simplified considering the matrix logarithm approximation [24, Chapter 3.2][31] $1/2(\mathbf{R}-\mathbf{R}^\top)$ in place of $\log(\mathbf{R}) = \theta/2\sin(\theta)(\mathbf{R}-\mathbf{R}^\top)$ that saves computational efforts, resulting in the displacement vector

$$\boldsymbol{h}(\mathbf{H}) := \frac{1}{2}\begin{bmatrix}(\mathbf{I}+\mathbf{R}^\top)\mathbf{o}\\ (\mathbf{R}-\mathbf{R}^\top)^\vee\end{bmatrix} \approx \begin{bmatrix}\frac{1}{2}(\mathbf{I}+\mathbf{R}^\top)\mathbf{o}\\ \log(\mathbf{R})^\vee\end{bmatrix} \tag{33}$$

yielding $P_0(\mathbf{H}) = 1/2\,\boldsymbol{h}^\top(\mathbf{H})\,\mathbf{K}\,\boldsymbol{h}(\mathbf{H})$ or explicitly

$$P_0(\mathbf{H}) = \frac{1}{2}\begin{bmatrix}1/2(\mathbf{I}+\mathbf{R}^\top)\mathbf{o}\\ 1/2(\mathbf{R}-\mathbf{R}^\top)^\vee\end{bmatrix}^\top \mathbf{K}\begin{bmatrix}1/2(\mathbf{I}+\mathbf{R}^\top)\mathbf{o}\\ 1/2(\mathbf{R}-\mathbf{R}^\top)^\vee\end{bmatrix}, \tag{34}$$

which is (14). The port-indifference of this potential energy function is quickly verified by noting that $\boldsymbol{h}(\mathbf{H}^{-1}) = -\boldsymbol{h}(\mathbf{H})$.

B. Derivation of the spring wrench

The wrench describing the spring forces and moments can be obtained by partially differentiating the elastic potential energy function with respect to the degrees of freedom. To write down the partial derivative of (34), we need to know the partial derivative of the 6D displacement vector $\boldsymbol{h}$ at $\mathbf{H}$ in an arbitrary direction $T_{\mathbf{H}}\mathrm{SE}(3) \ni \delta\mathbf{H} := \mathbf{H}\mathbf{v}^\wedge$, that we write $D\boldsymbol{h}(\mathbf{H})\cdot\delta\mathbf{H} = D\boldsymbol{h}(\mathbf{H})\cdot\mathbf{H}\mathbf{v}^\wedge$ [32], with $\mathbf{v} = [\boldsymbol{v};\boldsymbol{\omega}] \in \mathbb{R}^6$ the parameterization of the direction $\delta\mathbf{H}$ using a twist (an element of the Lie algebra of SE(3) in vector form). Recalling the expression for $\boldsymbol{h}$ given in (34), we get

$$\begin{aligned} D\boldsymbol{h}(\mathbf{H})\cdot\mathbf{H}\mathbf{v}^\wedge &= \frac{1}{2}\begin{bmatrix}(\mathbf{R}\boldsymbol{\omega}^\wedge)^\top\mathbf{o} + (\mathbf{I}+\mathbf{R}^\top)\mathbf{R}\boldsymbol{v}\\ (\mathbf{R}\boldsymbol{\omega}^\wedge - (\mathbf{R}\boldsymbol{\omega}^\wedge)^\top)^\vee\end{bmatrix} \\ &= \frac{1}{2}\begin{bmatrix}(\boldsymbol{\omega}^\wedge)^\top\mathbf{R}^\top\mathbf{o} + (\mathbf{I}+\mathbf{R}^\top)\mathbf{R}\boldsymbol{v}\\ (\boldsymbol{\omega}^\wedge\mathbf{R}^\top + \mathbf{R}\boldsymbol{\omega}^\wedge)^\vee\end{bmatrix} \\ &= \frac{1}{2}\begin{bmatrix}(\mathbf{R}^\top\mathbf{o})^\wedge\boldsymbol{\omega} + (\mathbf{R}+\mathbf{I})\boldsymbol{v}\\ (tr(\mathbf{R}^\top)(\boldsymbol{\omega})^\wedge - (\mathbf{R}^\top\boldsymbol{\omega})^\wedge)^\vee\end{bmatrix} \\ &= \frac{1}{2}\begin{bmatrix}(\mathbf{R}^\top\mathbf{o})^\wedge\boldsymbol{\omega} + (\mathbf{R}+\mathbf{I})\boldsymbol{v}\\ (tr(\mathbf{R})\mathbf{I} - \mathbf{R}^\top)\boldsymbol{\omega}\end{bmatrix} \\ &= \frac{1}{2}\begin{bmatrix}(\mathbf{R}+\mathbf{I}) & (\mathbf{R}^\top\mathbf{o})^\wedge\\ \mathbf{0}_{3\times3} & tr(\mathbf{R})\mathbf{I}-\mathbf{R}^\top\end{bmatrix}\underbrace{\begin{bmatrix}\boldsymbol{v}\\ \boldsymbol{\omega}\end{bmatrix}}_{=\mathbf{v}}, \end{aligned} \tag{35}$$

and $\boldsymbol{\omega}^\wedge\mathbf{R} + \mathbf{R}^\top\boldsymbol{\omega}^\wedge = tr(\mathbf{R})\boldsymbol{\omega}^\wedge - (\mathbf{R}\boldsymbol{\omega})^\wedge$ (cf., e.g., [33]). Knowing $D\boldsymbol{h}(\mathbf{H})\cdot\mathbf{H}\mathbf{v}^\wedge$, it is straightforward to compute the partial derivative of (34) in the direction $\mathbf{H}\mathbf{v}^\wedge$, namely

$$DP_0(\mathbf{H})\cdot\mathbf{H}\mathbf{v}^\wedge = \boldsymbol{h}(\mathbf{H})^\top\mathbf{K}\,D\boldsymbol{h}(\mathbf{H})\cdot\mathbf{H}\mathbf{v}^\wedge = \\ \underbrace{\frac{1}{4}\begin{bmatrix}(\mathbf{I}+\mathbf{R}^\top)\mathbf{o}\\ (\mathbf{R}-\mathbf{R}^\top)^\vee\end{bmatrix}^\top \mathbf{K}\begin{bmatrix}(\mathbf{R}+\mathbf{I}) & (\mathbf{R}^\top\mathbf{o})^\wedge\\ \mathbf{0}_{3\times3} & tr(\mathbf{R})\mathbf{I}-\mathbf{R}^\top\end{bmatrix}}_{=-_{S_1}(\mathbf{f}_{SPRG})_{L_2\to L_1}\text{(as a row vector)}}\mathbf{v}, \tag{36}$$

which is equivalent to (17), besides a transposition and a minus sign (as in standard Lagrangian mechanics, the force applied is given by minus the derivative of the potential).

APPENDIX B
PROOF OF PROPOSITION 1

The starting point of the proposition is assuming

$$P_0(\mathbf{H}) = P_0(\mathbf{T}_\theta^{-1}\mathbf{H}\mathbf{T}_\theta) \tag{37}$$

for any $\mathbf{H} \in \mathrm{SE}(3)$ and $\theta \in [0, 2\pi)$ with $\mathbf{T}_\theta$ defined as in (20) and $P_0(\mathbf{H})$ as in (14) or equivalently in (34). We have

$$\mathbf{T}_\theta^{-1}\mathbf{H}\mathbf{T}_\theta = \begin{bmatrix}\mathbf{R}_z^\top\mathbf{R}\mathbf{R}_z & \mathbf{R}_z^\top\mathbf{o}\\ \mathbf{0}_{1\times3} & 1\end{bmatrix}, \tag{38}$$

with $\mathbf{R}_z$ meaning $\mathbf{R}_z(\theta)$. Recalling the definition of $\mathbf{h}(\mathbf{H})$ in (34) and the identity $(\mathbf{R}\mathbf{u})^\wedge = \mathbf{R}\mathbf{u}^\wedge\mathbf{R}^\top$ for any $\mathbf{u} \in \mathbb{R}^3$ and $\mathbf{R} \in \mathrm{SO}(3)$, we get

$$\begin{aligned} 2\boldsymbol{h}(\mathbf{T}_\theta^{-1}\mathbf{H}\mathbf{T}_\theta) &= \begin{bmatrix}(\mathbf{I}+\mathbf{R}_z^\top\mathbf{R}^\top\mathbf{R}_z)\mathbf{R}_z^\top\mathbf{o}\\ (\mathbf{R}_z^\top\mathbf{R}\mathbf{R}_z - \mathbf{R}_z^\top\mathbf{R}^\top\mathbf{R}_z)^\vee\end{bmatrix} \\ &= \begin{bmatrix}\mathbf{R}_z^\top(\mathbf{I}+\mathbf{R}^\top)\mathbf{o}\\ \mathbf{R}_z^\top(\mathbf{R}-\mathbf{R}^\top)^\vee\end{bmatrix} = 2\mathbf{X}_{-\theta}\,\boldsymbol{h}(\mathbf{H}) \end{aligned} \tag{39}$$

where the twist coordinate transformation $\mathbf{X}_{-\theta} = \mathbf{X}_\theta^\top$, with

$$\mathbf{X}_\theta := \begin{bmatrix}\mathbf{R}_z & \mathbf{0}_{3\times3}\\ \mathbf{0}_{3\times3} & \mathbf{R}_z\end{bmatrix}. \tag{40}$$

From (39), the constraint (37) can be rewritten as

$$\boldsymbol{h}(\mathbf{H})^\top\mathbf{K}\boldsymbol{h}(\mathbf{H}) = \boldsymbol{h}(\mathbf{H})^\top\mathbf{X}_\theta\,\mathbf{K}\,\mathbf{X}_{-\theta}\,\boldsymbol{h}(\mathbf{H}). \tag{41}$$

Because $\boldsymbol{h}(\mathbf{H})$ is arbitrary and we must have $\mathbf{K} = \mathbf{X}_\theta\,\mathbf{K}\,\mathbf{X}_{-\theta}$ for any $\theta \in [0, 2\pi)$, leading to the conditions

$$\mathbf{K}_t = \mathbf{R}_z\mathbf{K}_t\mathbf{R}_z^\top, \tag{42}$$

$$\mathbf{K}_c = \mathbf{R}_z\mathbf{K}_c\mathbf{R}_z^\top, \tag{43}$$

$$\mathbf{K}_c^\top = \mathbf{R}_z\mathbf{K}_c^\top\mathbf{R}_z^\top, \text{ and} \tag{44}$$

$$\mathbf{K}_o = \mathbf{R}_z\mathbf{K}_o\mathbf{R}_z^\top. \tag{45}$$

Since $\mathbf{K}_t$ and $\mathbf{K}_o$ are symmetric, the previous conditions for $\mathbf{R}_z$ are satisfied if and only if

$$\mathbf{K}_t = \begin{bmatrix}k_{t_{xx}} & 0 & 0\\ 0 & k_{t_{xx}} & 0\\ 0 & 0 & k_{t_{zz}}\end{bmatrix} \text{ and} \tag{46}$$

$$\mathbf{K}_o = \begin{bmatrix}k_{o_{xx}} & 0 & 0\\ 0 & k_{o_{xx}} & 0\\ 0 & 0 & k_{o_{zz}}\end{bmatrix}. \tag{47}$$

Finally, as elements of $\mathbf{K}_c$ can assume any values, (43) and (44) can be satisfied if and only if

$$\mathbf{K}_c = \begin{bmatrix} k_{c_{xx}} & k_{c_{xy}} & 0 \\ -k_{c_{xy}} & k_{c_{xx}} & 0 \\ 0 & 0 & k_{c_{zz}} \end{bmatrix}. \tag{48}$$

This leads to the structure of the stiffness matrix $\mathbf{K}$ as given in the proposition statement. This concludes the proof.

Appendix C
Proof of Proposition 2

Let $\mathbf{e}_1, \mathbf{e}_2 \in \mathbb{R}^3$ be two orthogonal unit vectors and define $\mathbf{e}_3 = \mathbf{e}_1 \times \mathbf{e}_2$. An arbitrary translation vector in the $\mathbf{e}_1\mathbf{e}_2$-plane can be written as $\bar{\mathbf{o}}(\alpha, \beta) = \alpha\mathbf{e}_1 + \beta\mathbf{e}_2$, with $\alpha, \beta \in \mathbb{R}$, while a rotation orthogonal to the $\mathbf{e}_1\mathbf{e}_2$-plane can be written as $\bar{\mathbf{R}}(\gamma) = \mathbf{R}_{\mathbf{e}_3}(\gamma)$, with $\gamma \in \mathbb{R}$. Let

$$S = \{(\mathbf{o}, \mathbf{R}) \in \mathrm{SE}(3) : (\mathbf{o} = \bar{\mathbf{o}}(\alpha, \beta), \mathbf{R} = \bar{\mathbf{R}}(\gamma)); \alpha, \beta, \gamma \in \mathbb{R}\}$$

be the subgroup of SE(3) of all in-plane rigid transformation in the $\mathbf{e}_1\mathbf{e}_2$-plane. Let

$$V = \{\mathbf{v} \in \mathbb{R}^6 : \mathbf{v} = [\alpha\mathbf{e}_1 + \beta\mathbf{e}_2; \gamma\mathbf{e}_3]\},$$

that is $V \subset \mathbb{R}^6$ is the span of the 6D vectors $[\mathbf{e}_1; \mathbf{0}_{3\times1}]$, $[\mathbf{e}_2; \mathbf{0}_{3\times1}]$ and $[\mathbf{0}_{3\times1}; \mathbf{e}_3]$.

Let us consider the deformation vector $\boldsymbol{h}$ appearing in (33). By inspecting the expression of $\boldsymbol{h}(\mathbf{H})$ in (33), it is straightforward to see that

$$\forall \mathbf{H} \in S \implies \boldsymbol{h}(\mathbf{H}) \in V.$$

This should not be fully surprising since $\boldsymbol{h}(\mathbf{H})$ can be thought of an approximation of the logarithm on SE(3), mapping the $SE(3)$ to its Lie algebra, sharing the same property (on its domain of definition).

Given the above implication, it follows that V is an invariant subspace for the linear map $D\boldsymbol{h}(\mathbf{H}) \cdot \mathbf{H} : \mathbb{R}^6 \to \mathbb{R}^6$, for any fixed $\mathbf{H} \in S$. We recall that $D\boldsymbol{h}(\mathbf{H}) \cdot \mathbf{H}$ is derived in (35) and used to compute the spring wrench (36).

Let V^* denote the dual vector space of V, the vector space of wrenches generated by the 6D covectors that are dual to $[\mathbf{e}_1; \mathbf{0}_{3\times1}]$, $[\mathbf{e}_2; \mathbf{0}_{3\times1}]$ and $[\mathbf{0}_{3\times1}; \mathbf{e}_3]$. For duality, we have that V^* is an invariant subspace for $(D\boldsymbol{h}(\mathbf{H}) \cdot \mathbf{H})^\top$, the dual of $D\boldsymbol{h}(\mathbf{H}) \cdot \mathbf{H}$, for any fixed $\mathbf{H} \in \mathrm{SE}(3)$.

By assumption, a deformation $\mathbf{H} \in \mathrm{SE}(3)$ such that the translation happens in a plane which contains the z-axis (the axis of symmetry of the spring at rest) and the rotation $\mathbf{R}$ is orthogonal to that plane, must generate a force in the same plane and a torque along the plane's normal. Mathematically, recalling the derivation (36), this condition just expressed in words about the force and torque directions for any in-plane displacement $\mathbf{H} \in S$, can be written as

$$(D\boldsymbol{h}(\mathbf{H}) \cdot \mathbf{H})^\top \mathbf{K}\mathbf{h}(\mathbf{H}) \in V^*, \tag{49}$$

taking $\mathbf{e}_2$ to be the z-axis (the axis of symmetry of the spring at rest) and, without loss of generality, $\mathbf{e}_1$ to be the y-axis (and thus $\mathbf{e}_3$ being the x-axis).

Remarkably, $D\boldsymbol{h}(\mathbf{H}) \cdot \mathbf{H}$ and thus $(D\boldsymbol{h}(\mathbf{H}) \cdot \mathbf{H})^T$ are invertible given the fact that $\mathbf{h}(\mathbf{H})$ is a local diffeomorphism. This, combined with the invariance of V^* with respect to $(D\boldsymbol{h}(\mathbf{H}) \cdot \mathbf{H})^\top$, leads to the implication

$$(D\boldsymbol{h}(\mathbf{H}) \cdot \mathbf{H})^\top \mathbf{K}\mathbf{h}(\mathbf{H}) \in V^* \implies \mathbf{K}\mathbf{h}(\mathbf{H}) \in V^*.$$

Because $\mathbf{H} \in S$ implies that $\boldsymbol{h}(\mathbf{H}) \in V$, sticking to the illustrative example $\mathbf{e}_1 = y$, $\mathbf{e}_2 = z$, and $\mathbf{e}_3 = x$, it follows that $\mathbf{K}\boldsymbol{h}(\mathbf{H})$ must be a linear combination of the second, third, and fourth columns of $\mathbf{K}$ in (21). Namely, these columns are

$$\begin{array}{c} \\ x \to \\ y \to \\ z \to \\ x \circlearrowleft \\ y \circlearrowleft \\ z \circlearrowleft \end{array} \begin{array}{c} \begin{array}{ccc} y \to & z \to & x \circlearrowleft \end{array} \\ \begin{bmatrix} 0 & 0 & k_{c_{xx}} \\ k_{t_{xx}} & 0 & -k_{c_{xy}} \\ 0 & k_{t_{zz}} & 0 \\ -k_{c_{xy}} & 0 & k_{o_{xx}} \\ k_{c_{xx}} & 0 & 0 \\ 0 & k_{c_{zz}} & 0 \end{bmatrix} \end{array}, \tag{50}$$

where the symbols $\to$ and $\circlearrowleft$ represent translation and rotation components, respectively. The 3×3 gray submatrix appearing above represents the in-plane stiffness matrix. It is evident that for a linear combination of the columns of (50) to be always in V^*, the terms $k_{c_{xx}}$ and $k_{c_{zz}}$ appearing in the first, fifth, and sixth rows must then be zero. This shows that the matrix $\mathbf{K}$ must have the structure (22), given in the proposition statement. This concludes the proof.

References

[1] X. Cheng, Y. Hou, and M. T. Mason, "Manipulation with suction cups using external contacts," in *Robotics Research*, T. Asfour, E. Yoshida, J. Park, H. Christensen, and O. Khatib, Eds. Cham: Springer International Publishing, 2022, pp. 692–708.

[2] C. Correa, J. Mahler, M. Danielczuk, and K. Goldberg, "Robust toppling for vacuum suction grasping," in *2019 IEEE 15th International Conference on Automation Science and Engineering (CASE)*, 2019, pp. 1421–1428.

[3] R. Shome, W. N. Tang, C. Song, C. Mitash, H. Kourtev, J. Yu, A. Boularias, and K. E. Bekris, "Towards robust product packing with a minimalistic end-effector," in *2019 International Conference on Robotics and Automation (ICRA)*, 2019, pp. 9007–9013.

[4] J. Mahler, M. Matl, X. Liu, A. Li, D. Gealy, and K. Goldberg, "Dex-net 3.0: Computing robust vacuum suction grasp targets in point clouds using a new analytic model and deep learning," in *2018 IEEE International Conference on Robotics and Automation (ICRA)*, 2018, pp. 5620–5627.

[5] F. Gabriel, M. Fahning, J. Meiners, F. Dietrich, and K. Dröder, "Modeling of vacuum grippers for the design of energy efficient vacuum-based handling processes," *Production Engineering*, vol. 14, no. 5, pp. 545–554, Dec 2020. [Online]. Available: https://doi.org/10.1007/s11740-020-00990-9

[6] Q. Shao, J. Hu, W. Wang, Y. Fang, W. Liu, J. Qi, and J. Ma, "Suction grasp region prediction using self-supervised learning for object picking in dense clutter," *2019 IEEE 5th International Conference on Mechatronics System and Robots (ICMSR)*, pp. 7–12, 2019.

[7] W. Shuai, Y. Gao, P. Wu, G. Cui, Q. Zhuang, R. Chen, and X. Chen, "Compliant-based robotic 3d bin packing with unavoidable uncertainties," *IET Control Theory & Applications*, Jan 2023.

[8] N. Correll, K. E. Bekris, D. Berenson, O. Brock, A. Causo, K. Hauser, K. Okada, A. Rodriguez, J. M. Romano, and P. R. Wurman, "Analysis and observations from the first amazon picking challenge," *IEEE Transactions on Automation Science and Engineering*, vol. 15, no. 1, pp. 172–188, 2018.

[9] K.-T. Yu and A. Rodriguez, "Realtime state estimation with tactile and visual sensing for inserting a suction-held object," in *2018 IEEE/RSJ International Conference on Intelligent Robots and Systems (IROS)*, 2018, pp. 1628–1635.

[10] G. A. Fontanelli, G. Paduano, R. Caccavale, P. Arpenti, V. Lippiello, L. Villani, and B. Siciliano, "A reconfigurable gripper for robotic autonomous depalletizing in supermarket logistics," *IEEE Robotics and Automation Letters*, vol. 5, no. 3, pp. 4612–4617, 2020.

[11] F. Raptopoulos, M. Koskinopoulou, and M. Maniadakis, "Robotic pick-and-toss facilitates urban waste sorting," in *2020 IEEE 16th International Conference on Automation Science and Engineering (CASE)*, 2020, pp. 1149–1154.

[12] B. Bahr, Y. Li, and M. Najafi, "Design and suction cup analysis of a wall climbing robot," *Computers & Electrical Engineering*, vol. 22, no. 3, pp. 193–209, 1996.

[13] J. Liu, K. Tanaka, L. Bao, and I. Yamaura, "Analytical modelling of suction cups used for window-cleaning robots," *Vacuum*, vol. 80, no. 6, pp. 593–598, 2006.

[14] G. Mantriota, "Theoretical model of the grasp with vacuum gripper," *Mechanism and Machine Theory*, vol. 42, no. 1, pp. 2–17, 2007.

[15] ——, "Optimal grasp of vacuum grippers with multiple suction cups," *Mechanism and Machine Theory*, vol. 42, no. 1, pp. 18–33, 2007.

[16] H. Pham and Q.-C. Pham, "Critically fast pick-and-place with suction cups," in *2019 International Conference on Robotics and Automation (ICRA)*, 2019, pp. 3045–3051.

[17] N. Dehio and A. Kheddar, "Robot-safe impacts with soft contacts based on learned deformations," in *2021 IEEE International Conference on Robotics and Automation (ICRA)*, 2021, pp. 1357–1363.

[18] A. Bernardin, C. Duriez, and M. Marchal, "An interactive physically-based model for active suction phenomenon simulation," in *2019 IEEE/RSJ International Conference on Intelligent Robots and Systems (IROS)*, 2019, pp. 1466–1471.

[19] J. Hudoklin, S. Seo, M. Kang, H. Seong, A. T. Luong, and H. Moon, "Vacuum suction cup modeling for evaluation of sealing and real-time simulation," *IEEE Robotics and Automation Letters*, vol. 7, no. 2, pp. 3616–3623, 2022.

[20] Y. Karako, T. Moriya, M. Abe, H. Shimakawa, S. Shirahori, and Y. Saitoh, "A practical simulation method for pick-and-place with vacuum gripper," in *2017 56th Annual Conference of the Society of Instrument and Control Engineers of Japan (SICE)*, 2017, pp. 1351–1356.

[21] E. D. Fasse and P. C. Breedveld, "Modeling of Elastically Coupled Bodies: Part I—General Theory and Geometric Potential Function Method," *Journal of Dynamic Systems, Measurement, and Control*, vol. 120, no. 4, pp. 496–500, 12 1998. [Online]. Available: https://doi.org/10.1115/1.2801491

[22] M. Lubbers, J. van Voorst, M. Jongeneel, and A. Saccon, "Learning suction cup dynamics from motion capture: Accurate prediction of an object's vertical motion during release," in *2022 IEEE/RSJ International Conference on Intelligent Robots and Systems (IROS)*, 2022, pp. 1541–1547.

[23] S. Traversaro and A. Saccon, *Multibody dynamics notation (version 2)*. Technische Universiteit Eindhoven, Nov. 2019, dept. of Mechanical Engineering. Report locator DC 2019.100.

[24] R. M. Murray, S. S. Sastry, and L. Zexiang, *A Mathematical Introduction to Robotic Manipulation*. CRC Press, Inc., 1994.

[25] K. M. Lynch and F. C. Park, *Modern Robotics: Mechanics, Planning, and Control*, 1st ed. New York, NY, USA: Cambridge University Press, 2017.

[26] M. L. Hage, "Data collection for suction cup modelling at varying internal pressure," Eindhoven, January 2023, available at https://pure.tue.nl/ws/portalfiles/portal/293049172/1246704_BEP_Report_Max_Hage.pdf.

[27] E. D. Fasse and P. C. Breedveld, "Modeling of Elastically Coupled Bodies: Part II—Exponential and Generalized Coordinate Methods," *Journal of Dynamic Systems, Measurement, and Control*, vol. 120, no. 4, pp. 501–506, 12 1998. [Online]. Available: https://doi.org/10.1115/1.2801492

[28] *schmalz VS...SA Vacuum/pressure sensor product description.*, schmalz, 2016. [Online]. Available: https://pimmedia.schmalz.com/MAM_Library/Dokumente/Bedienungsanleitung/30/3030/303001/30300100955/BAL_30.30.01.00955_en-EN.pdf

[29] M. Jongeneel and A. Saccon, "Geometric Savitzky-Golay Filtering of Noisy Rotations on SO(3) with Simultaneous Angular Velocity and Acceleration Estimation," in *2022 IEEE/RSJ International Conference on Intelligent Robots and Systems (IROS)*, 2022, pp. 2962–2968.

[30] F.-G. Wieland, A. L. Hauber, M. Rosenblatt, C. Tönsing, and J. Timmer, "On structural and practical identifiability," *Current Opinion in Systems Biology*, vol. 25, pp. 60–69, 2021.

[31] Y. Wang and G. S. Chirikjian, "Nonparametric second-order theory of error propagation on motion groups," *The International Journal of Robotics Research*, vol. 27, no. 11-12, pp. 1258–1273, 2008, pMID: 20333324. [Online]. Available: https://doi.org/10.1177/0278364908097583

[32] J. E. Marsden and T. S. Ratiu, *Introduction to Mechanics and Symmetry*, 2nd ed. New York, NY, USA: Texts in Applied Mathematics, Springer, 1999.

[33] G. Gallego and A. Yezzi, "A compact formula for the derivative of a 3-d rotation in exponential coordinates," *Journal of Mathematical Imaging and Vision*, vol. 51, no. 3, pp. 378–384, Mar 2015. [Online]. Available: https://doi.org/10.1007/s10851-014-0528-x